Int J Adv Manuf Technol (2007) 33: 266–276
DOI 10.1007/s00170-006-0456-z

ORIGINAL ARTICLE

Rosendo Zamora · Félix Faura · Joaquín López · Julio Hernández

Experimental verification of numerical predictions for the optimum plunger speed in the slow phase of a high-pressure die casting machine

Received: 20 June 2005 / Accepted: 30 December 2005 / Published online: 5 May 2006

Abstract An experimental study of the optimum maximum plunger speed in the slow phase of a high-pressure die casting machine with horizontal cold chamber is presented. A special apparatus that uses a photoelectric sensor to determine the instant at which the working fluid reaches the runner was developed and installed in the injection chamber. The measured volumes of air remaining in the chamber at this instant for various maximum plunger speeds were compared with those predicted by a three-dimensional numerical model based on a finite element formulation and the volume of fluid method for treating the free surface. Very good agreement was found between experimental and numerical results, except for maximum plunger speeds higher than the optimal, for which very complex fluid flow phenomena (that would require a more detailed numerical analysis of the air entrapment mechanisms) tend to be produced. The optimum maximum plunger speed at which the measured volume of trapped air is minimum was found to be very close to that predicted numerically.

Keywords Air entrapment · High-pressure die casting machine · Maximum plunger speed · Porosity · Slow phase

Nomenclature

A	Cross-sectional area of the injection chamber
A_l	Cross-sectional area occupied by the liquid
c	Speed relative to the fluid of a small-amplitude wave corresponding to A_l
f	Initial filling fraction, A_{l0}/A
g	Gravitational acceleration
h	Free-surface height
H	Height of the injection chamber
l	Length in the plunger acceleration law of Eq. (2)
L	Length of the injection chamber
n	Number of measurements during a shot
R^2	Statistical coefficient of determination
t	Time
t_e	Time delay of the signal emitted by the photoelectric sensor
t_f	Filling time of the injection chamber
t_m	Time at which the control system detects the signal emitted by the photoelectric sensor
t_p	Actual time at which the liquid begins to flow through the runner
t_H	Time at which the plunger acceleration ceases
T	Width of the free surface
U_{max}	Maximum plunger speed in the slow phase
V	Volume of air remained in the chamber at the instant t_p
x,y,z	Coordinates (Fig. 7)
X	Location of the plunger face

Subscripts

0	Quantity corresponding to the initial depth

R. Zamora · F. Faura · J. López (✉)
Departamento de Ingeniería de Materiales y Fabricación,
ETSII, Universidad Politécnica de Cartagena,
C/ Dr. Fleming, s/n,
30202 Cartagena, Spain
e-mail: joaquin.lopez@upct.es
Tel.: +34-968-325962
Fax: +34-968-326445

J. Hernández
Departamento de Mecánica, ETSII, UNED,
28040 Madrid, Spain

1 Introduction

High-pressure die casting (HPDC) using machines with horizontal cold chambers (currently the most commonly used in processes for manufacturing near-net shape cast components) allows very high production rates with small dimensional tolerances and a good surface finish. The most common defect in the parts manufactured by this process is porosity, one important cause of which is the entrapment of air during injection [1]. The selection of appropriate operating conditions during injection can contribute to

minimizing such porosity and, to this end, the injection process usually consists of slow and fast shot phases (see, respectively, Fig. 1(a) and (b)). This work focuses on the slow initial phase, during which the plunger first forces the molten metal to rise and fill the upper section of the injection chamber, and then moves at a constant speed until the molten metal completely fills the injection chamber. The amount of air trapped during this initial phase may represent a considerable contribution to the total mass of trapped air that produces porosity in the manufactured part. This is particularly so when inappropriate operating parameters are used during injection.

Air entrapment in the injection chamber is related to the behavior of the surface wave of the molten metal caused by plunger motion. If the plunger reaches a speed higher than a certain optimum value, the wave will reflect against the chamber ceiling, as shown in Fig. 2(b), and its forward face might roll over; or, the ceiling jet formed might reach the runner too early, both of which cause air to be trapped. On the other hand, if the plunger speed does not reach this optimum value, the wave might reflect against the end wall of the chamber and trap air in front of the plunger and along the chamber ceiling, as shown in Fig. 2(a). Different authors (see, for example, references [2–8]) carried out experiments using water as working fluid in a transparent injection chamber and visualization techniques to analyze the influence of different injection conditions on air entrapment effects during the slow phase. In particular, Garber [3] studied experimentally the existence of a critical plunger speed above which the impact of the metal against the chamber ceiling causes the wave to roll over. The studies of Karni [4], Duran et al. [5] and Brevick et al. [6] mainly focused on the influence of the plunger acceleration law on the amount of air trapped in the chamber. They used a photo-cell switch to determine the instant at which the water completely covers the chamber end wall, and related the air remaining in the chamber at this instant to the air trapped during the slow phase. The studies devoted to

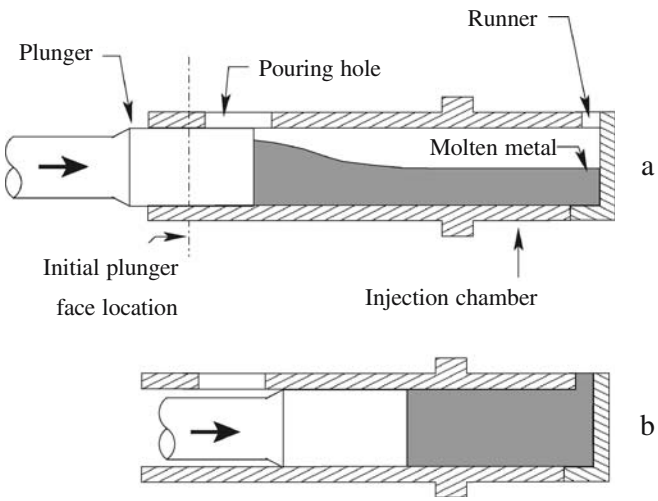

Fig. 1 Schematic representation of the injection chamber of an HPDC machine during (**a**) the initial slow stage and (**b**) the subsequent fast stage of the injection process

investigating experimentally the flow of molten metal in real operating conditions are relatively scarce. Although authors such as Smith and Wallace [9], Lindsey and Wallace [10], Brevick et al. [11] and Huang et al. [12] made experiments in HPDC machines with cold chambers, their results are mainly related with the fast injection phase.

Theoretical investigations aimed at determining a suitable plunger motion law may be mostly classified into analytical [3, 11, 13, 14–17] or numerical [18–24] approaches. Backer and Sant [19] used the Wrafts code [25] to simulate the fluid flow of molten metal in the injection chamber. This code, which is based on a finite element formulation to solve the momentum and mass conservation equations and a volume of fluid (VOF) method to describe the free surface, was also used by López et al. [22] to obtain the optimum maximum plunger speed for different initial filling fractions and plunger acceleration laws. The simulations were carried out without considering the reflection of the wave of molten metal against the chamber end wall, which in our previous works had been taken into account only for two-dimensional chamber configurations [20, 21]. The possibility of estimating the optimum plunger speed using simple models based on the one-dimensional shallow-water approximation was also investigated in [22]. A detailed description of these simpler models can be found in [15, 16, 22].

In this work, the optimum maximum plunger speed that minimizes air entrapment in the chamber is determined experimentally in a real die casting machine. A plunger acceleration law proposed by López et al. [16], which attempts to reduce air entrapment effects, was used in all the experiments. A special apparatus that uses a photo-electric sensor was installed in the machine to measure the instant at which the working fluid (water) reaches the runner. The volume of air remaining in the chamber at this instant is determined as a function of the maximum plunger speed for different initial filling fractions. The experimental results are compared with those obtained with a three-dimensional numerical model, similar to that used by López et al. [22], but taking into account the reflection of the wave against the chamber end wall in order to quantify the volume of trapped air in the chamber. For validation purposes, the results of the numerical model are also compared with those obtained with a simplified shallow-water model. The results of this work have allowed us to assess experimentally the possibilities and limitations of using the numerical model as a useful tool in the design of appropriate operating conditions.

2 Experimental procedure

2.1 Equipment and instrumentation

The experiments were carried out in an HPDC machine with horizontal cold injection chamber and a locking force of 1500 kN, using water as the working fluid. A sketch of the machine is represented in Fig. 3, where the moving and fixed parts of the die are open. The special apparatus

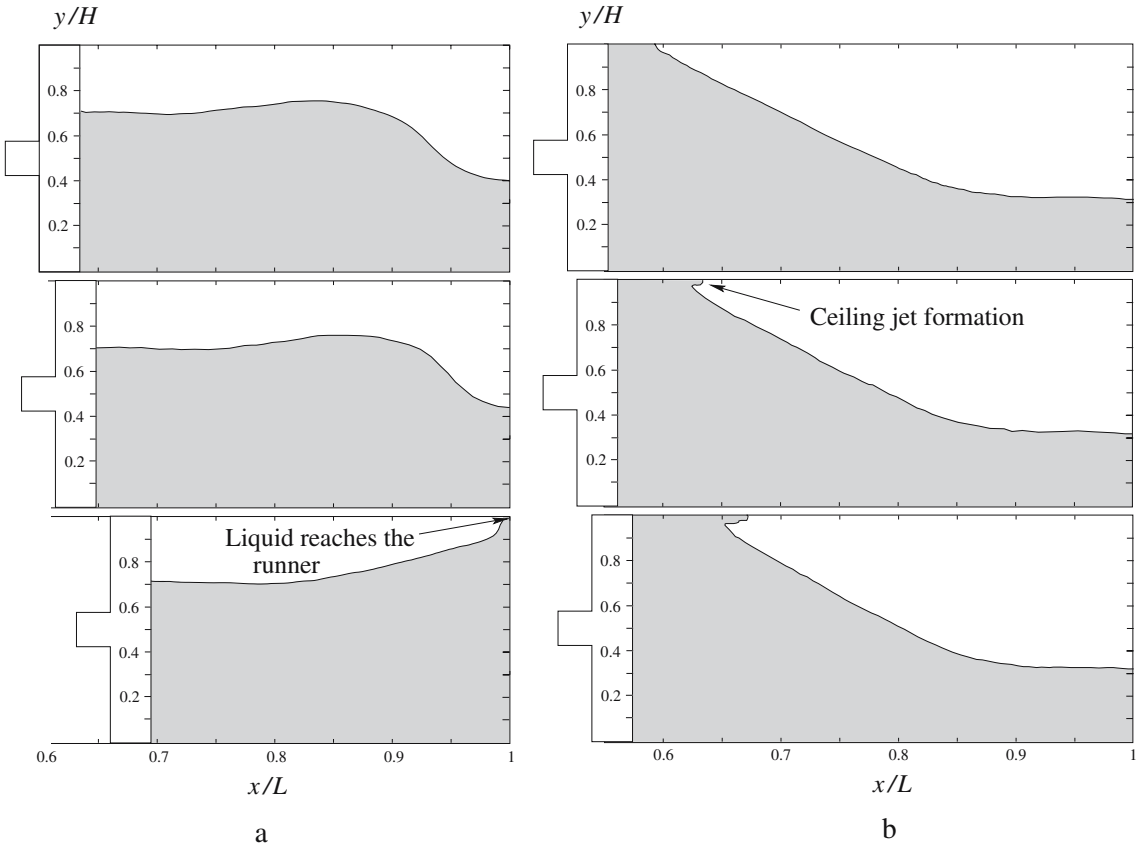

Fig. 2 Simulation results of two cases with maximum plunger speeds lower (**a**) and higher (**b**) than the optimal speed that minimizes the volume of trapped air in the injection chamber (wave surface profiles at the symmetry plane of the injection chamber)

installed on the moving side of the die, shown in more detail in Fig. 4, includes a thin runner, which is open to the atmosphere and allows the correct evacuation of the air contained in the chamber, and the device used to determine the instant at which the water begins to flow through the runner, which generates the light signal that activates a photoelectric sensor. The thickness of the runner was made equal to the diameter of the fiber-optic cable (1.2 mm) connected to the photoelectric sensor. Some tests were performed with colored water, and no appreciable differences were observed in the determination of this instant.

A schematic representation of the control system of the machine is shown in Fig. 5. A programmable logic control system regulates the plunger motion at ten different positions along the total stroke using a hydraulic system with a proportional central control valve. The opening percentages of the valve can be adjusted between 10 and 100% by means of a PC-based interface. It should be

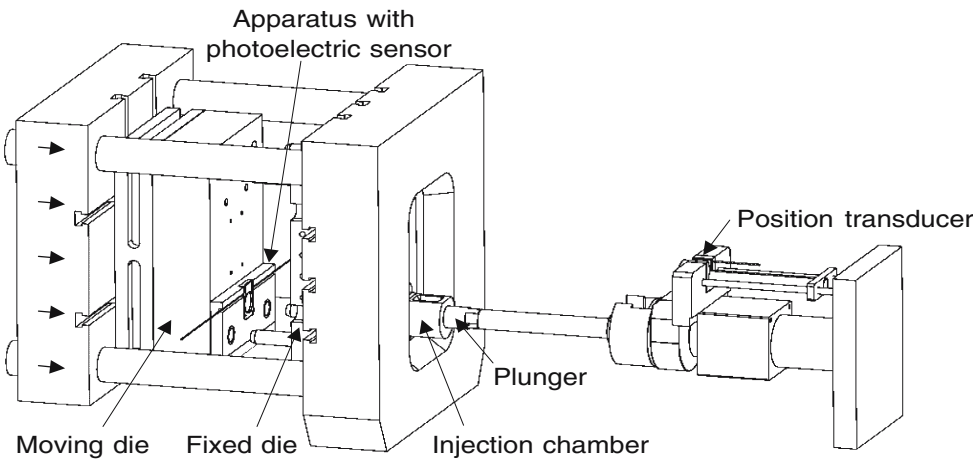

Fig. 3 Sketch of the HPDC machine

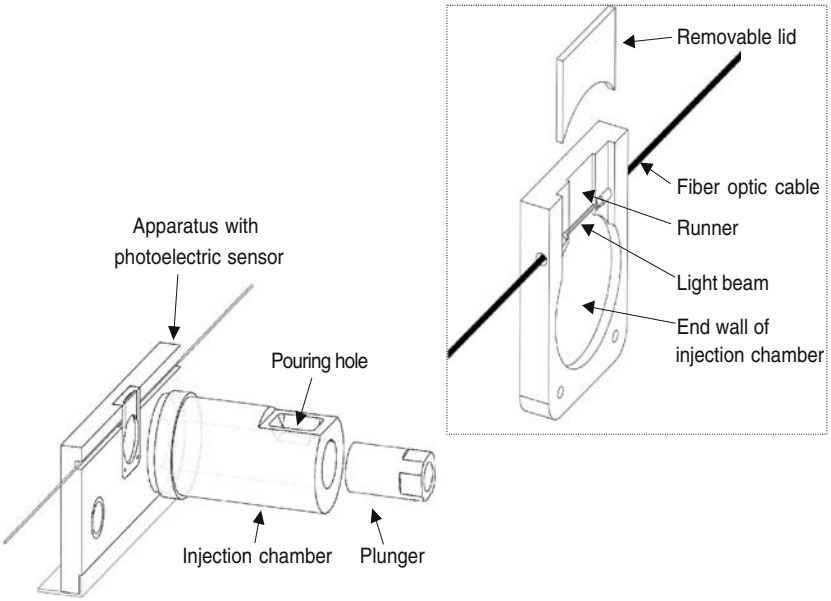

Fig. 4 3D view of the special apparatus that incorporates the runner and the device used to detect the flow of water through the runner

mentioned that the required values of the opening percentages of the valve to reproduce a certain plunger motion law depend on several variables: initial filling fraction, plunger diameter, chamber length, pressure and temperature of the hydraulic system, and friction effects between the plunger and the injection chamber, among others. The appropriate values of the valve opening were adjusted using a trial-and-error procedure with the aid of a computer code specifically developed for this purpose. The position of the plunger face at any time t, $X(t)$, was measured using a magneto-resistive position transducer that generates a digital signal with a resolution of 0.1 mm and a manufacturer-specified maximum error of ±0.1 mm. In order to check the accuracy of the position transducer, different measurements were carried out by programming the machine in order to stop the plunger at different locations. The difference between the registered plunger position at a given location and that obtained with a high-precision measurement instrument (with a resolution of 0.01 mm) was found to be always lower than the maximum error mentioned above.

When the plunger speed measured during a given shot did not follow the desired law closely enough, the injection experiment was rejected. These cases were detected when the statistical coefficient of determination

$$R^2 = 1 - \frac{\sum_{i=1}^{n}\left(X_i' - \widehat{X}_i'\right)^2}{\sum_{i=1}^{n}\left(X_i' - \overline{X}'\right)^2} \quad (1)$$

was lower than 0.9 (n is the number of measurements, X_i' and $\widehat{X}_i'$ are the measured and the desired plunger speed, and $\overline{X}'$ the mean value of the plunger speed during the shot). Table 1 shows the number of shots performed and rejected for the different operating conditions used in the experiments. It should be mentioned that 86% of all injection shots for which $R^2 \geq 0.9$ had an R^2 coefficient greater than 0.95. As an example, the relatively good degree of agreement between the desired (continuous line) and measured (dotted line) plunger speeds for a typical shot with $R^2=0.95$ can be observed in Fig. 6.

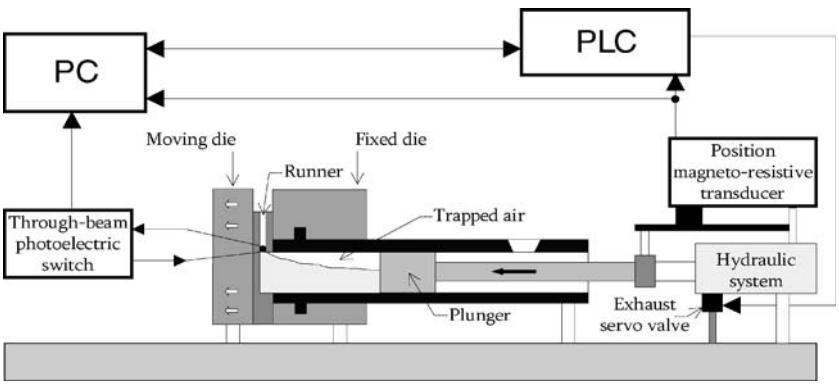

Fig. 5 Schematic representation of the control system installed in the HPDC machine

Table 1 Ranges of operating conditions used in the experiments and corresponding number of performed and rejected shots

	Initial filling fraction, A_{l0}/A		
	0.252	0.374	0.5
Range of maximum plunger speeds, $U_{max}/(gH)^{1/2}$	0.41÷1.21	0.45 ÷ 1.27	0.36 ÷ 1.09
Number of performed shots	146	142	129
Number of rejected shots	1	21	35

Experiments were carried out for the three initial filling fractions of Table 1, which required using ladles of different volumes. The ladles were calibrated using a high-precision balance (resolution of 10^{-4} g and repeatability of $\pm 2\times10^{-4}$ g). The maximum error in the volume of water poured into the chamber was found to be around ±0.2 per cent of the total volume of the injection chamber (AL). The initial length and diameter of the chamber used were L=0.265 m and H=0.05 m, respectively, which gave a relation L/H=5.3. For each combination of initial filling fraction and maximum plunger speed values, a series of at least ten injection shots was carried out. The following plunger acceleration law [16, 17] was used:

$$X''(t) = \frac{2}{3}\frac{c_0^2}{l}\left[1 - \frac{c_0}{l}t\right]^{-4/3}, \text{ for } t \le t_H \qquad (2)$$

where (t_H is the time at which the plunger acceleration ceases $X''(t) = 0$ for $t>t_H$), l is a positive constant and $c_0 = (gA_{l0}/T_0)^{1/2}$ is the speed relative to the fluid of a small-amplitude wave (g is the gravitational acceleration, A_{l0} the cross-sectional area initially filled with liquid, and T_0 the corresponding width of the free surface; see Fig. 7). The injection shot was stopped when the plunger reached a position (which depends on the initial filling fraction) that ensured water had started to flow through the runner. After each injection, the runner was blown with compressed air in order to clean out the light beam area.

2.2 Experimental determination of the volume of trapped air

Each shot was initiated a certain time after the water was poured manually in order to allow the liquid in the chamber to come to rest, and the free surface to become (within reason) flat. The volume of air remaining in the injection chamber at the instant t_p at which the water begins to flow through the runner, made dimensionless with the initial chamber volume, is given by:

$$\frac{V}{AL} = \frac{L - X(t_p)}{L} - f, \qquad (3)$$

where $X(t_p)$ is the length traveled by the plunger at the instant t_p and $f=A_{l0}/A$ is the initial filling fraction (note that the remaining volume in the chamber at the instant t_p is $A(L - X(t_p))$ and the volume of poured water is ALf). It is expected that this volume is related to the volume of air trapped within the liquid and that a considerable fraction of the porosity of the manufactured part is caused by this trapped air.

The injection control system provided discretized data of the plunger position X and the state of the photoelectric sensor ('off' in the normal state and 'on' when the water has reached the runner) as a function of time t, with a sampling frequency of about 10,000 data per second. The plunger speed X' at any time was calculated from the discretized plunger positions using a time-centered finite difference formula. The time interval of differentiation was sufficient to avoid spurious errors due to the limited resolution of the position transducer. The maximum error of the plunger speed obtained in this way was estimated to be in the order of ±0.003 ms^{-1}

In order to determine the plunger position at the instant at which the water begins to flow through the runner, it is necessary to estimate the slight time delay produced in the transmission of the signal from the photoelectric sensor to the control system. For this purpose, a test was carried out in which the photoelectric sensor was used to detect the moment a fixed reference mark made in the plunger crossed the light beam, when the plunger was moved with different constant speeds X' (in the range between 0.16 and 0.81 ms^{-1}). Figure 8 shows the plunger position registered by the magneto-resistive transducer, $X(t_m)$, corresponding to the instant at which the control system registers the crossing of the reference mark, t_m, as a function of the plunger speed, $X'(t_m)$. Note that, if the time delay of the signal, t_e, is constant, $X(t_m)$ must increase linearly with the plunger speed, and so the actual position of the sensor can be estimated as $X(t_m) - t_e X'(t_m)$. The signal delay was obtained as the slope of the linear correlation curve through the experimental points (with a correlation coefficient of 0.997), which was calculated to

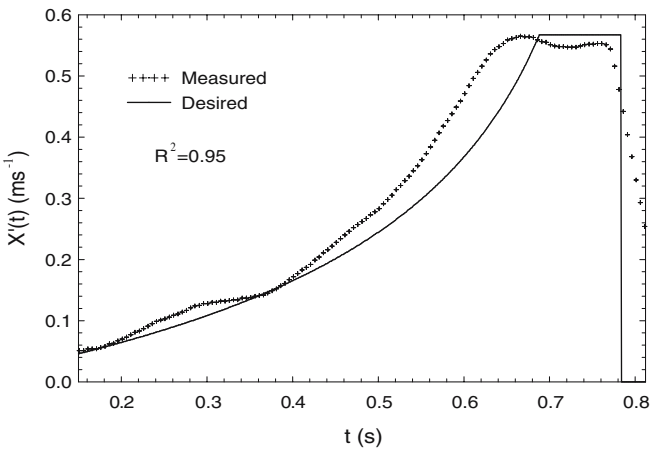

Fig. 6 Comparison between theoretical (continuous line) and measured (cross symbols) plunger speeds for a typical shot with R^2=0.95 (A_{l0}/A=0.374 and U_{max}=0.57 ms^{-1})

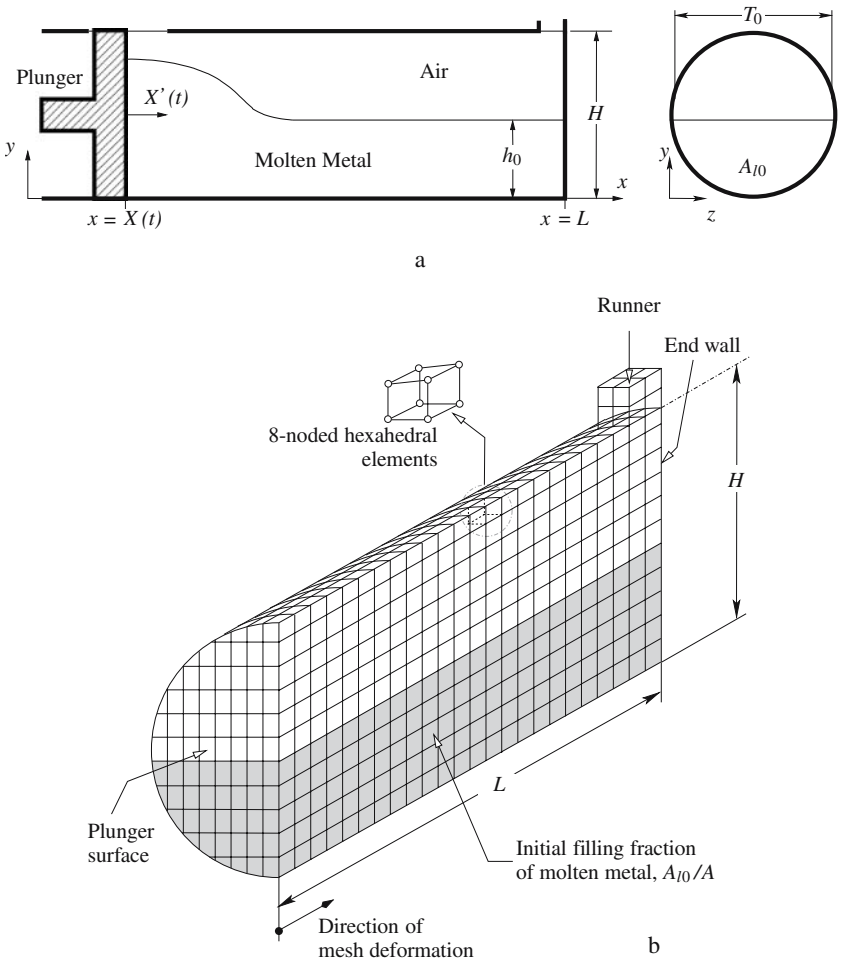

Fig. 7 (**a**) Schematic representation of the chamber and coordinate system. (**b**) Sketch of the grid used in the 3D numerical model

be t_e=1.32±0.01 ms. Then, if t_m is the time at which the control system detects the signal emitted by the photoelectric sensor after the water begins to flow through the runner, the actual plunger position $X(t_p)$ in Eq. (3) is obtained from

$$X\left(t_p\right) = X(t_m) - t_e X^{'}(t_m) \tag{4}$$

where $X(t_m)$ is the plunger position registered by the magneto-resistive transducer and $X^{'}(t_m)$ the corresponding plunger speed.

3 Numerical models

3.1 CFD model

The results for the amount of trapped air in the injection chamber are compared in Section 4 with those predicted by a three-dimensional CFD code (Wrafts code [25]), which is based on a finite element method to solve the momentum and mass conservation equations using a projection method [26]. The momentum equations were solved using an explicit time integration for the velocities, and the pressure was calculated from a Poisson equation at each time step. A volume of fluid (VOF) method [27] was used to describe the evolution of the free surface, and the mesh was moved and deformed using a technique similar to the arbitrary Lagrangian–Eulerian method [28]. The nodes located at the plunger face were moved according to the law of Eq. (2), and those at the chamber end wall were maintained in a fix position. The influence of air motion on the dynamics of the free surface has been neglected, and so

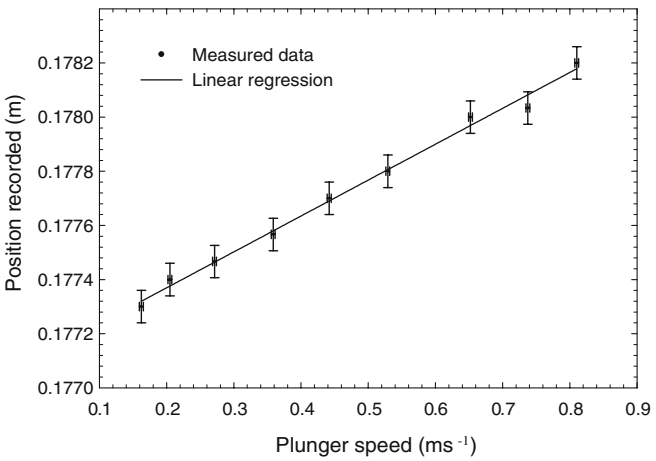

Fig. 8 Signal time delay correlation

only the flow in the liquid phase was solved. As mentioned in the Introduction, López et al. [22] already applied this model to study the flow in a chamber of circular cross section, but without considering effects of wave reflection against the end wall of the injection chamber.

It will be considered that the liquid in the chamber is initially at rest and that the free surface is flat (Fig. 7). Heat transfer and solidification effects are neglected (the typical duration of the slow injection phase is in the order of 1 s). Because of the symmetry of the problem, only one half of the physical domain is solved. A computational mesh with 8-noded hexahedral elements is used (Fig. 7(b)), except at the cylindrical chamber wall, where some of the elements have six nodes.

The pressure in the free surface cells is fixed, and a no-slip condition is imposed at the injection chamber walls. At the plunger face, the horizontal velocity given by the acceleration law of Eq. (2) is fixed. Appropriate boundary conditions were imposed at the symmetry plane. Attention in this work was focused on conditions close to the optimal, for which surface tension effects are expected to have very little influence on the free-surface dynamics; they have therefore been neglected. Operating conditions far from the optimal, for which phenomena such as those involved in wave breaking processes or wall jet formation occur at very early stages of the shot, are not considered. Additional numerical details of the code are given in [21] (where a comparison with some experimental data is made) and [22].

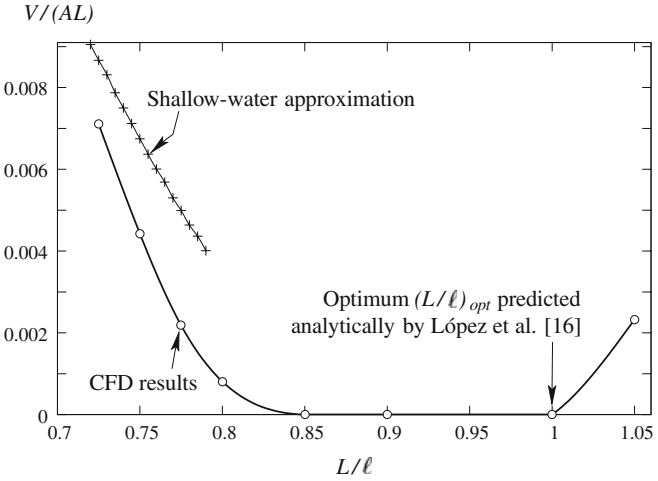

Fig. 10 Dimensionless volume $V/(AL)$ as a function of L/l for the same chamber dimensions and initial filling fraction of Fig. 9, and using the maximum plunger speed proposed by López et al. [22] to avoid wall jet formation along the chamber ceiling

3.2 One-dimensional shallow-water model

In this section, the simplified model of the flow in the injection chamber based on the shallow-water approximation will be briefly described. In this model, viscous effects and vertical acceleration will be neglected, so that hydrostatic conditions will prevail along any vertical line in the liquid (further details can be found in references [21, 22]; a detailed analysis about the validity of the shallow-water approximation for typical operating conditions can be found in reference [21]). By using the method of characteristics, the governing equations reduce to the following compatibility conditions:

$$\frac{du}{dt} \pm \frac{g}{c}\frac{dh}{dt} = 0, \tag{5}$$

along the characteristic lines defined by

$$\frac{dx}{dt} = u \pm c, \tag{6}$$

where $h=h(x,t)$ is the free-surface height, $u=u(x,t)$ is the horizontal velocity component of liquid, $A_l=A_l(x,t)$ is the cross-sectional area filled with liquid, $T=T(x,t)$ is the width of the free surface, g is the gravitational acceleration, and $c = (gA_l/T)^{1/2}$ is the speed relative to the fluid of a small amplitude wave corresponding to the area A_l (the coordinate system is represented in Fig. 7(a)). It is considered that the liquid in the injection chamber is initially at rest, and that the area occupied by the liquid is a given fraction, A_{l0}/A, of the cross-sectional area of the chamber. A boundary condition is applied at the plunger surface, where the

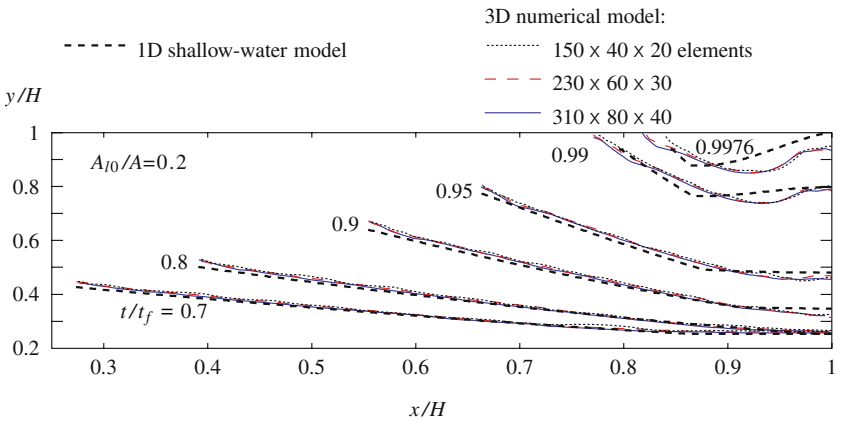

Fig. 9 Wave surface profiles at the symmetry plane of an injection chamber with L/H=9 and H=0.05 m, for an initial filling fraction A_{l0}/A=0.2, the plunger acceleration law of Eq. (2) with l=4/3 L, and the maximum plunger speed limit given by López et al. [22] to avoid wall jet formation along the chamber ceiling

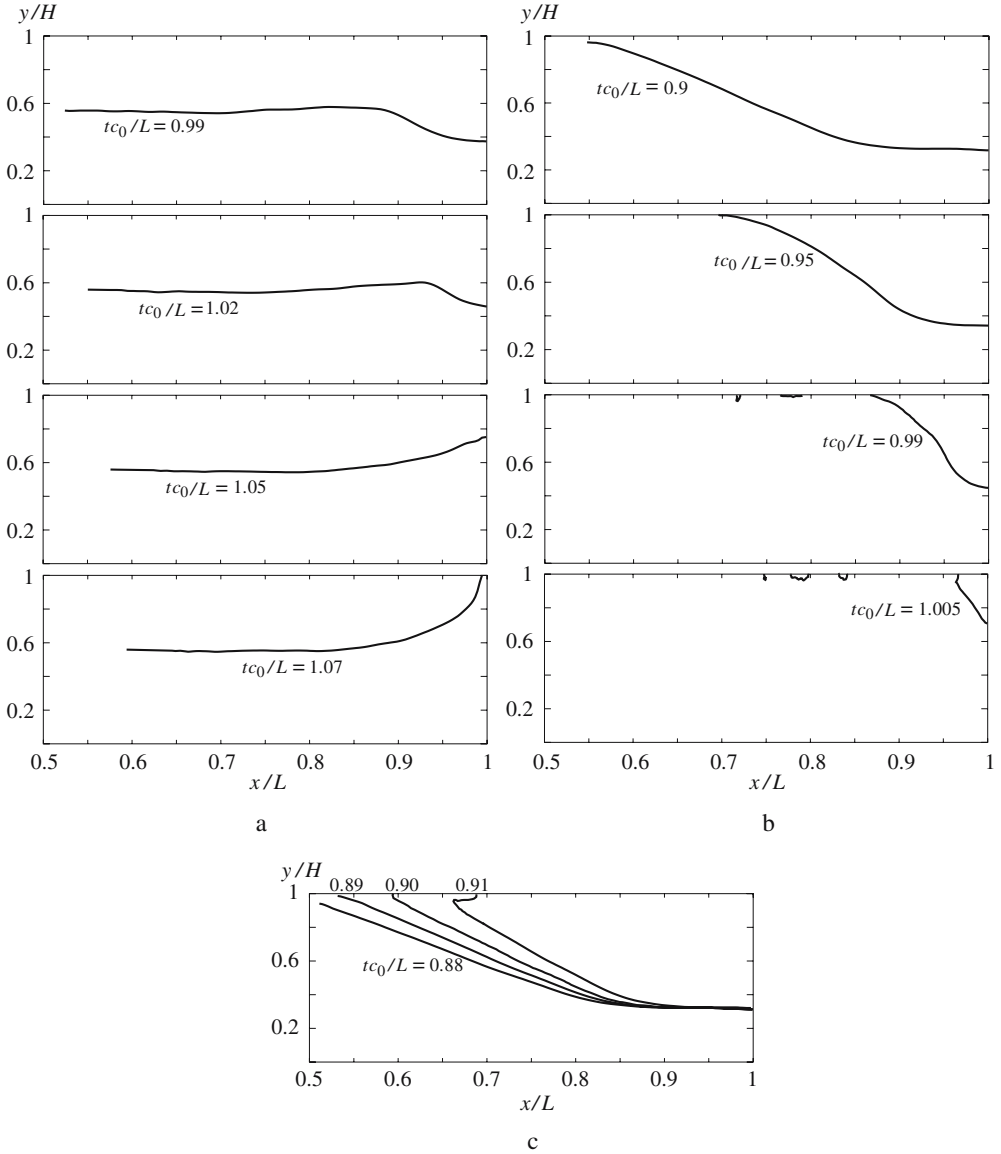

Fig. 11 Results of the CFD model for the wave surface profiles in the symmetry plane of the chamber, for L=5.3 H, H=0.05 m, A_{l0}/A=0.252, the plunger acceleration law of Eq. (2), and different maximum dimensionless plunger speeds $U_{max}/(gH)^{1/2}$: (**a**) 0.42; (**b**) 0.88; (**c**) 1.0

velocity of liquid is taken to be equal to the plunger velocity given by Eq. (2). To take into account the effect of wave reflection against the end wall of the chamber, another boundary condition is applied at this wall, where u is taken equal to zero.

Unlike when the chamber is considered to be two-dimensional and wave reflection effects are neglected, Eqs. (5) and (6) have no analytical solution and must be solved numerically. The numerical resolution is carried out using a deformable finite difference grid in the x-t plane and an algorithm based on the inverse marching method, in which the locations of solution points are specified a priori. The characteristic curves through each solution point are extended rearward to intersect the line of constant time on which the points calculated at the previous time step are located. The characteristic curves between the solution point and the intersection points (initial data points) are approximated by straight lines. The finite difference equations resulting from the discretization of Eqs. (5) and (6) are solved by using the modified Euler predictor-corrector method. In the predictor step, the coefficients in the finite difference equations are calculated at the initial-data points, where the flow properties are determined from a natural cubic spline interpolation based on previous solution points. In the corrector step, the coefficients are calculated from the average values of the dependent variables along each characteristic curve. At each time step, a uniform grid step size Δx is calculated, and a ratio $\Delta x/\Delta t$ is chosen to satisfy the CFL stability condition.

4 Results and discussion

4.1 Comparison between results of the CFD and shallow-water models

The results of the CFD model and of the shallow-water model presented in the previous section were first

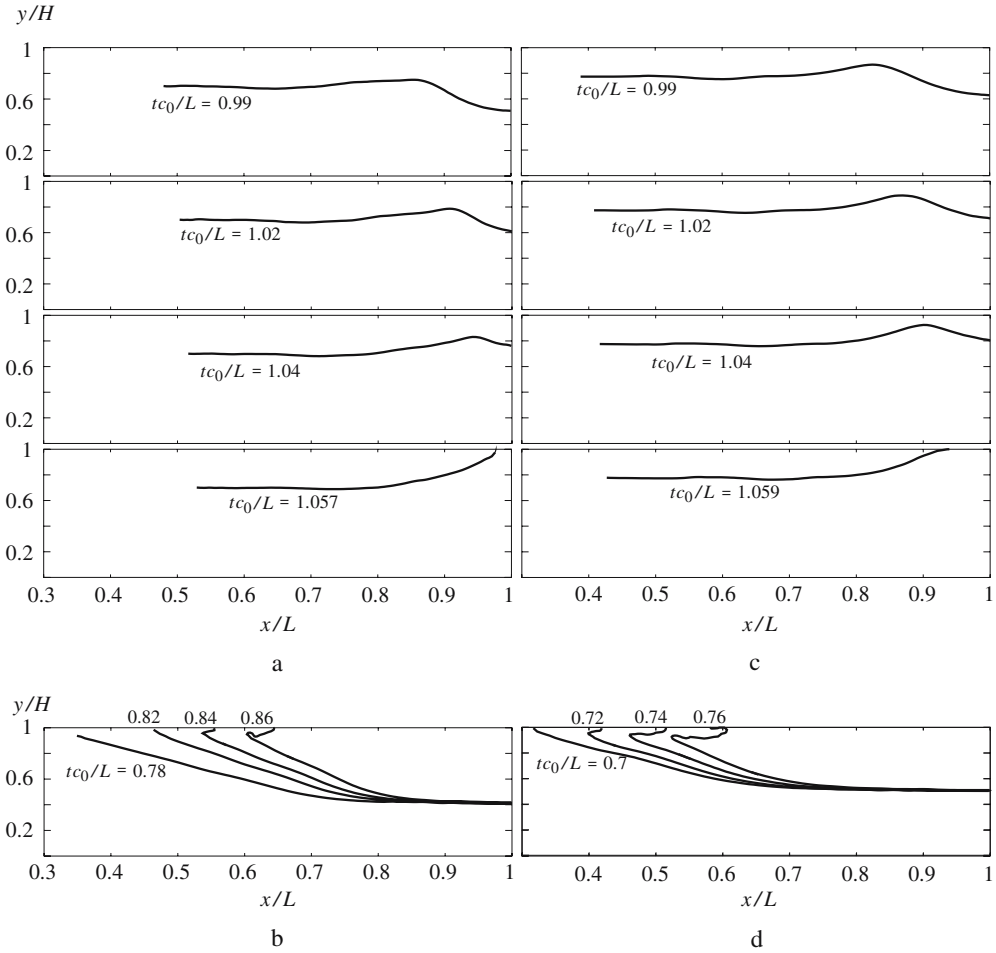

Fig. 12 Results of the CFD model for the wave surface profiles in the symmetry plane of the chamber, for L=5.3H, H=0.05 m, the plunger acceleration law of Eq. (2), two different initial filling fractions and maximum dimensionless plunger speeds $U_{max}/(gH)^{1/2}$: (**a**) 0.43 and (**b**) 0.74 for A_{l0}/A=0.374; and (**c**) 0.35 and (**d**) 0.62 for A_{l0}/A=0.5

compared for injection conditions involving a relatively intense reflection of the metal wave against the end wall of the chamber, corresponding to a sufficiently high value of the parameter l in Eq. (2) ($l = 4/3L$). As an example, Fig. 9 shows results for the wave surface profile at the symmetry plane of an injection chamber with L=9H, H=0.05 m and a low initial filling fraction, A_{l0}/A=*0.2*. The results of the CFD model were obtained with grids of three different sizes, using the dynamic viscosity and density of pure aluminum at its freezing point (1.3×10^{-3} Pa s and 2385 kg m^{-3}, respectively). The vertical scale of the figure has been enlarged by a factor of 2.34 in order to emphasize the differences between both types of results. The time has been made dimensionless with the time

$$t_f = t_H + \frac{L(1-f) - X(t_H)}{U_{\max}}, \tag{7}$$

at which the injection chamber would be completely filled with liquid (filling time). U_{max} is the maximum speed reached by the plunger (i.e., $X'(t)$=U_{max} for t>t_H). In order to avoid the formation of a ceiling jet in the CFD simulation, plunger acceleration ceased when its speed reached the optimum maximum value predicted by López et al. [22] (it can be noted from the figure that the height of the free surface predicted by the 1D model reaches a maximum value of y/H=0.94 in the last two profiles depicted). Also, note that near grid-independent results are obtained for mesh sizes in the range considered in Fig. 9. The rest of the results presented in this work were obtained with the intermediate mesh of 230×60×30 elements. On the other hand, a very good agreement can be observed from Fig. 9 between the wave profiles predicted by the 1D and 3D models, even for the last instants represented. Notice, however, that the shallow-water model predicts a slightly earlier closure of the runner, which, in this case, is caused by the reflection of the wave against the end wall.

To avoid air entrapment as a result of wave reflection against the end wall of the chamber, a plunger acceleration higher than that corresponding to Fig. 9 should be used (note that the lower the l value, the higher the plunger acceleration). Figure 10 shows CFD and shallow-water results for the dimensionless volume *V/(AL)* occupied by the air in the injection chamber when the liquid reaches the runner, as a function of the non-dimensional acceleration parameter L/l, for the same chamber dimensions and initial filling fraction of Fig. 9. For L/l values higher than around 0.8, the shallow-water model predicts that the wave will break before the liquid reaches the runner, and so only CFD results are represented. For L/l<0.8, note that the earlier closure of the runner predicted by the shallow-water model

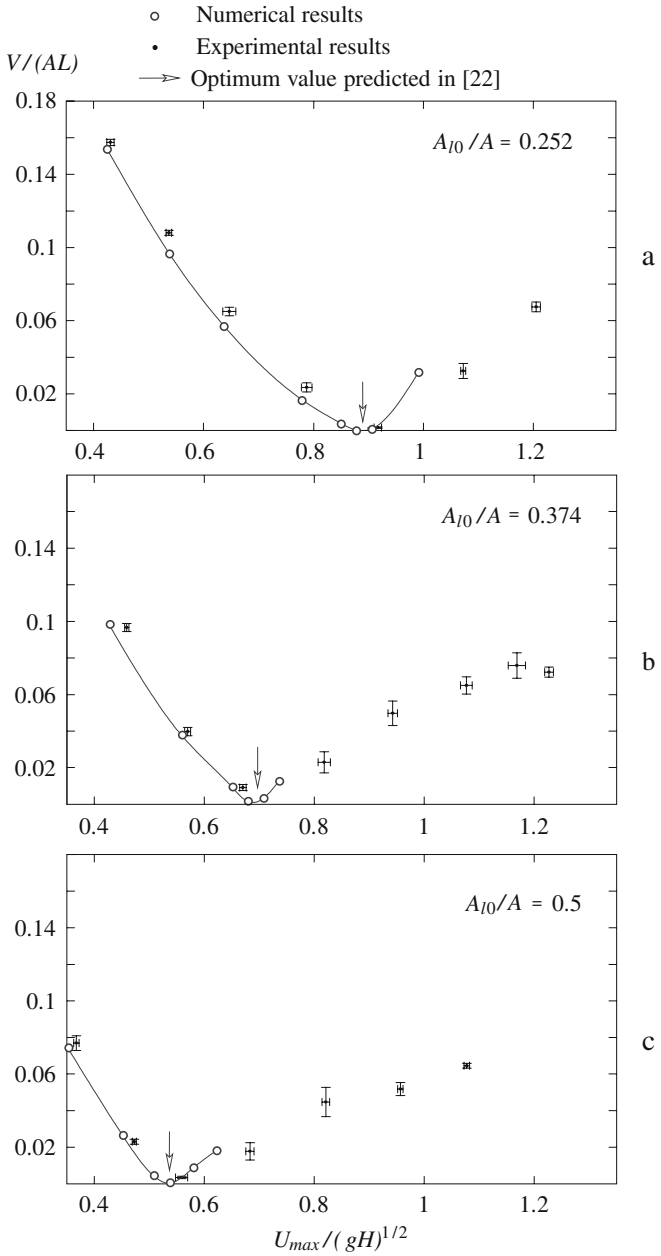

Fig. 13 Experimental and numerical results for the dimensionless volume $V/(AL)$ as a function of the maximum dimensionless plunger speeds $U_{max}/(gH)^{1/2}$, for the same plunger acceleration law of Figs. 11 and 12 and different initial filling fractions. The vertical arrows represent the optimum values predicted numerically by López et al. [22]

mentioned above produces higher volumes of trapped air than those obtained with the CFD model. It can be observed that the optimum value of L/l which minimizes air entrapment while keeping the chamber filling time as low as possible (t_f decreases as L/l increases) is very close to the optimum value $(L/l)_{opt}=1$ predicted analytically by the shallow-water model for an equivalent chamber with a two-dimensional cross-section configuration [16].

4.2 Comparison with the experimental results

Experimental observations by Garber [3] and the numerical predictions carried out by López et al. [22] showed that, for certain injection conditions, a wall jet tends to be formed along the chamber ceiling, which results in the overturning of the free surface. It was suggested that the wall jet could be avoided, or its effects minimized, by stopping the plunger acceleration at a certain instant before the liquid completely covers the plunger face. Figure 11, which corresponds to an initial filling fraction of 0.252, and Figs. 12(a,b) and 12(c,d), for initial filling fractions of 0.374 and 0.5, respectively, show the numerical results for the wave surface profiles at the symmetry plane obtained with the three-dimensional CFD model for different maximum plunger speeds and the same chamber configuration as used in the experiments, with H=0.05 m and L/H=5.3. The optimum plunger acceleration parameter, $l=L$, predicted analytically by López et al. [16], and the dynamic viscosity and density of water, were used in all computations presented in this section. It can be observed that, when the maximum plunger speed is too high (see Figs. 11(c), 12(b) and (d)), a wall jet is formed along the chamber ceiling, whereas when it is too low, the reflection of the wave against the end wall of the chamber tends to increase air entrapment (see the results for the lowest maximum plunger speed in each figure). The results of Fig. 11(b), corresponding to the optimum U_{max} value predicted numerically by López et al. [22], show that the wall jet along the chamber ceiling can be avoided and the amount of trapped air can be considerably reduced by stopping plunger acceleration at a certain time before the liquid completely covers the plunger face.

In Fig. 13 we compare numerical and experimental results for the dimensionless volume occupied by the air in the injection chamber at the instant at which the liquid begins to flow through the runner, $V/(AL)$. Figure 13(a–c) show, for initial filling fractions A_{l0}/A=0.252, 0.374, and 0.5, respectively, the mean value and 95% confidence interval of $V/(AL)$ as a function of the maximum plunger speed reached by the plunger, U_{max}. The confidence intervals were calculated from a Student's t distribution and taking into account the errors in the measurement of the plunger position, volume of poured liquid and time at which the liquid begins to flow through the runner. The 3D numerical results are represented in Fig. 13 with open circles. It can be observed that there is good quantitative agreement between the numerical and experimental results, except for plunger speeds higher than the optimal, for which the wall jet formation along the chamber ceiling would require a more detailed analysis of the flow, taking into account, for example, surface tension effects and using a higher grid resolution to simulate the small-scale motions which are expected to appear. It is worth noting that, for the operating conditions considered in the experiments, the volume of trapped air in the chamber, V, may reach values higher than ten percent of the total volume of the chamber AL. Also note that, for the optimum plunger acceleration parameter $l=L$ used in the experiments, there is an optimum

maximum plunger speed for which the volume of trapped air in the injection chamber is reduced to zero, even for the lower initial filling fraction used.

For each value of the initial filling fraction, Fig. 13 also shows, with a vertical arrow, the optimum maximum plunger speed predicted by López et al. [22] using the three-dimensional CFD model, but neglecting effects of wave reflection against the chamber end wall. Note that this value is very close to that corresponding to the minimum volume of trapped air obtained in this work, which confirms the fact that, in the range of plunger acceleration parameters considered in this figure, the formation of a wall jet along the chamber ceiling, rather than the effects of wave reflection against the chamber end wall, is the decisive factor that determines the optimum value of U_{max}.

5 Conclusions

The volume of air remaining in the injection chamber of a real die casting machine at the instant at which the liquid begins to flow through the runner has been measured for wide ranges of the maximum speed reached by the plunger and three different initial filling fractions. A three-dimensional numerical model, based on a finite element formulation and the volume of fluid method for treating the free surface, whose results were compared with the results of a shallow-water model, was used to simulate the flow in the injection chamber for the same experimental conditions in the die casting machine. The agreement between the measurements and the numerical predictions was very good for plunger speeds lower than the optimal. For higher speeds, complex fluid flow phenomena associated with the formation of a wall jet along the chamber ceiling would require a more detailed numerical analysis of the air entrapment mechanisms. The optimum maximum plunger speed for which the measured volume of trapped air is minimum was also found to be very close to that predicted by the numerical model. From these results, it can be concluded that the numerical model proposed in this work can be regarded as a useful prediction tool for the design of operating conditions that tend to reduce porosity in manufactured parts.

Acknowledgement The authors gratefully acknowledge the support of the Spanish Ministerio de Educación y Ciencia under Grants DPI2001-1390-C02 and DPI2004-08198.

References

1. Campbell J (1991) Castings. Butterworth-Heinemann, Oxford
2. Sheptak N (1963) Water analogue study of fluid flow in the cold chamber. AFS Trans 71:349–357
3. Garber LW(1982) Theoretical analysis and experimental observation of air entrapment during cold chamber filling. Die Cast Eng 26(3):14–22
4. Karni Y (1991) Selection of process variables for die casting. Dissertation, The Ohio State University
5. Duran M, Karni Y, Brevick JR, Chu Y, Altan T (1991) Minimization of air entrapment in the shot sleeve of a die casting machine to reduce porosity. Technical Report ERC/NSM-C-91-31, The Ohio State University
6. Brevick JR, Duran M, Karni Y (1991) Experimental determination of slow shot velocity-position profile to minimize air entrapment. SDCE Trans D-T91-0C4
7. Bennett CH (1987) Clear plastic model experiments-cold chamber analysis. SDCE Trans G-T87-016
8. Davis A, Asquith SJ (1985) Water analogue studies of fluid flow in the die casting process. SDCE Trans G-T85-063
9. Smith WE, Wallace JF (1963) Gating of die castings. AFS Trans 71:325–348
10. Lindsey D, Wallace JF (1972) Effect of vent size and design, lubrication practice, metal degassing, die texturing and filling of shot sleeve on die casting soundness. Trans 7th SDCE Int. Die Casting Congress and Exposition Chicago 10372:1–15
11. Brevick JR, Amentrout DJ, Chu Y (1994) Minimization of entrained gas porosity in aluminum horizontal cold chamber die castings. Trans NAMRI/SME 22:41–46
12. Huang YJ, Hu BH, Pinwill I, Zhou W, Taplin DMR (2000) Effects of process settings on the porosity levels of AM60B magnesium die castings. Mater Manuf Process 15:97–105
13. Thome MC, Brevick JR (1993) Modeling fluid flow in horizontal cold chamber diecasting shot sleeves. AFS Trans 101:343–348
14. Thome MC, Brevick JR (1995) Optimal slow shot velocity profiles for cold chamber die casting. NADCA Congress and Exposition. Indianapolis, T95-024
15. Tszeng TC, Chu YL (1994) A study of wave formation in shot sleeve of a die casting machine. J Eng Ind-T ASME 116 (2):175–182
16. López J, Hernández J, Faura F, Trapaga G (2000) Shot sleeve wave dynamics in the slow phase of die casting injection. J Fluid Eng-T ASME 122(2):349–356
17. Faura F, López J, Hernández J (2001) On the optimum plunger acceleration law in the slow shot phase of pressure die casting machines. Int J Mach Tool Manuf 41(2):173–191
18. Kuo TH, Hwang WS (1998) Flow pattern simulation in shot sleeve during injection of diecasting. AFS Trans 106:497–503
19. Backer G, Sant F (1997) Using finite element simulation for the development of shot sleeve velocity profiles. NADCA Congress and Exposition, Minneapolis, T97–014
20. Hernández J, López J, Gómez P, Faura F (1999) Influence of non-hydrostatic and viscous effects on shot sleeve wave dynamics in die casting injection. Proc 3rd ASME/JSME Joint Fluids Engineering Conference, F-209: Advances in Free Surface and Interface Fluid Dynamics, San Francisco, FEDSM99-7087, pp 248
21. Hernández J, López J, Faura F, Gómez P (2003) Analysis of the flow in the injection chamber of a high pressure die casting machine. J Fluid Eng-T ASME 125:315–324
22. López J, Faura F, Hernández J, Gómez P (2003) On the critical plunger speed and three-dimensional effects in high-pressure die casting injection chambers. J Manuf Sci E-T ASME 125:529–537
23. Khayat RE (1998) A three-dimensional boundary element approach to confined free-surface flow as applied to die casting. Eng Anal Bound Elem 22:83–102
24. Hernández J, Gómez P, Crespo A, López J, Faura F (2001) Breaking waves in a high-pressure die-casting injection chamber. In: Michaelides EE (ed), Proc 4th International Conference on Multiphase Flow, New Orleans, pp 898
25. Sant F, Backer G (1995) Application of WRAFTS fluid flow modeling software to the bench mark test casting. In: Cross M, Campbell J (eds) Modeling of casting, welding and advanced solidification processes VII. TMS, Warrendale, PA, pp 983–990
26. Chorin AJ (1969) On the convergence of discrete approximations of the Navier-Stokes equations. Math Comput 23:341–353
27. Hirt CW, Nichols BD (1981) Volume of fluid (VOF) method for the dynamics of free boundaries. J Comput Phys 39:201–225
28. Hirt CW, Amsden AA, Cook JL (1974) An arbitrary Lagrangian-Eulerian computing method for all flow speeds. J Comput Phys 14:227–253